Supercritical Airfoil Boundary-Layer and Near-Wake Measurements

D. A. Johnson*
NASA Ames Research Center, Moffett Field, California
and
F. W. Spaid†
McDonnell Douglas Corporation, St. Louis, Missouri

The flow behavior within the upper-surface boundary layer and near wake of a supercritical airfoil operating at cruise conditions is discussed. Experimental results obtained from wind tunnel tests are presented which provide a more detailed description of the flow in these regions than was previously available. Mean streamwise velocity profiles measured by pitot-pressure-probe and laser-velocimeter techniques were found to be in excellent agreement. Other mean-flow properties obtained by the laser-velocimeter technique were the local flow angles in the viscous layers and the static pressures at the edges of the boundary layer and wake. The data set also includes measurements of the turbulence intensity and turbulent Reynolds stress distributions as obtained by the laser-velocimeter technique. To assess the effects of the shock wave, a less extensive set of measurements was realized at a subcritical test condition. The two test conditions ($M_\infty = 0.72$, $C_L = 0.76$ and $M_\infty = 0.5$, $C_L = 0.75$) provide a good test for state-of-the-art prediction methods because the upper-surface boundary layer is separated just upstream of the trailing edge in both cases.

Nomenclature

c = chord length of airfoil
C_L = airfoil section lift coefficient
C_f = skin-friction coefficient $= \tau_w / \frac{1}{2}\rho_e u_e^2$
C_p = local pressure coefficient $= (p - p_\infty) / \frac{1}{2}\rho_\infty u_\infty^2$
H = boundary-layer shape factor
M = Mach number
N = total number of velocity realizations
p = static pressure
R_{uv} = uv correlation coefficient $= \overline{u'v'} / \langle u' \rangle \langle v' \rangle$
u = velocity component in streamwise direction
v = velocity component in normal direction
x = coordinate in the streamwise direction
y = coordinate in the normal direction
α = angle of attack
δ = viscous-layer thickness
δ_i^*, δ^* = kinematic and compressible boundary-layer displacement thicknesses, respectively
ϵ = turbulent eddy viscosity
Θ = flow angle = arctan $\bar{v}/\bar{u}$
θ = boundary-layer momentum thickness
ρ = fluid density
τ_w = wall shear stress
ω = weighting factor for velocity biasing

Subscripts and Superscripts

e = conditions at edge of viscous layer
i = ith velocity realization
∞ = freestream conditions
$(\,)'$ = fluctuating quantity
$\bar{(\,)}$ = time-averaged quantity
$\langle\, ' \,\rangle$ = rms value of quantity

Introduction

THE pronounced aft camber and flat upper surface of supercritical airfoil sections combine to make the performance of these airfoils very dependent on viscous effects. Even at the design Mach number and lift coefficient, the thickening of the upper-surface boundary layer near the trailing edge caused by the aft camber is sufficient to have a first-order effect on the surface-pressure distribution. A significant change in shock location can also occur because of the flat upper surface, which puts little constraint on the shock. Thus any feasible predictive method must accurately account for this boundary-layer growth. Because of the very strong adverse pressure gradients at the shock and near the trailing edge, however, the correct modeling of the boundary-layer growth is not trivial. Often there is a small region of separated flow near the trailing edge; although it is not large enough to affect performance, it does pose difficulties for the predictive method.

In addition to these boundary-layer effects, the performance of supercritical sections appears to be sensitive to the flow character in the near wake. It has been determined (by interferometry techniques) that there are significant static-pressure differences across the wake as far downstream as 10% chord of the trailing edge.[1] This was also observed in the present study. These static-pressure differences are attributed to wake-curvature effects, and it has been advocated that the correct modeling of these effects is also important in the prediction of surface-pressure distributions.[2,3]

Significant difficulties have arisen in developing accurate predictive methods for supercritical sections. Strongly debated is whether the unsatisfactory numerical solutions to date are results of improper turbulence closure models, inappropriate approximations in the numerical methods, inadequate spatial resolution (particularly of the solutions of the time-averaged Navier-Stokes equations), or of some combination thereof.

It is clear that there is a need for detailed measurements of the boundary layer and near-wake flowfields of supercritical sections at or near cruise conditions. Little such data exist and they are limited to mean measurements obtained with pressure probes. In this paper, experimental data obtained with a supercritical airfoil section at cruise conditions are presented;

Presented as Paper 81-1242 at the AIAA 14th Fluid and Plasma Dynamics Conference, Palo Alto, Calif., June 23-25, 1981; submitted Aug. 12, 1981; revision received July 12, 1982. This paper is declared a work of the U.S. Government and therefore is in the public domain.

*Research Scientist. Member AIAA.
†Senior Scientist, McDonnell Douglas Research Laboratories. Associate Fellow AIAA.

they include measurements of the turbulent-flow properties as well as mean-velocity measurements. Another unique feature of the results is that redundant measurements of the mean-velocity profiles were obtained with pitot-pressure-probe and laser-velocimeter techniques. These redundant measurements provide a degree of confidence in the mean-velocity measurements that was lacking in previous studies in which only pressure probes were used. The data also include the local flow angles, the turbulence intensities, and the Reynolds shear stresses as measured with the laser-velocimeter technique. For a point of reference, similar measurements were obtained with the laser velocimeter at a subcritical test condition.

Experimental Approach

The model used in the test program was a 14%-thick supercritical airfoil section (DSMA 671) with a 20.32-cm chord (aspect ratio of 3). This section is designed for a lower cruise Mach number ($M_\infty = 0.72$) than the 11%-thick DSMA 523 section used in the studies of Refs. 1 and 4. Another major difference in the two sections is that the DSMA 671 has a reduced adverse pressure gradient in the region of the lower-surface concavity; this eliminates the separated flow on the lower surface observed in the DSMA 523 experiments. The model, which had a relatively sharp trailing edge, was unconventional in that it had a constant-radius bow in the spanwise direction. The radius of the bow was 29 times the chord of the airfoil, which resulted in the upper surface being 1.56 cm higher at the tunnel centerline than at the sidewalls. This rather radical design was incorporated to facilitate the upper-surface boundary-layer measurements made with the laser velocimeter. As discussed in the Results section, the bow in the airfoil was sufficiently small so as not to degrade the spanwise uniformity of the flow.

The experiments were conducted in the 2×2-ft transonic wind tunnel at the Ames Research Center. The tunnel is a closed-return, variable-density type with 21% open porous-slotted upper and lower walls for transonic testing. The model spanned the test section and was pin-mounted to the optical glass windows of the solid, plane sidewalls. Changes in angle of attack were accomplished by rotation of these windows.

The tests were conducted at a chord Reynolds number of 3×10^6. To insure fully turbulent boundary layers, transition strips were located at 17% chord on both upper and lower surfaces.

Boundary-layer and near-wake pitot pressures were made with an 2-degree-of-freedom traversing rig and probe assembly; the rig and probe assembly was mounted on the tunnel sting support. The end of the single-orifice pitot probe was made from 0.81-mm-o.d. stainless steel tubing, flattened and ground at the tip to a height of 0.15 mm, with a 0.05-mm opening height and 0.05-mm walls. The traverse assembly was of a more recent design than that used in Ref. 4. The interference effects of the probe and the traverse assembly on the airfoil pressure distributions were observably less than those in the study of Ref. 4. For a discussion of these effects, the reader is referred to Ref. 4.

Measurements of the local static-pressure distributions with a static-pressure probe were not attempted since the accuracy of such measurements would have been highly suspect. This is due to the rapid changes in local flow angle that occur across the viscous layers and the sensitivity to alignment errors with the local flow of static-pressure probes. Instead, the static pressure was assumed to be constant across the viscous layers in the reduction of the pitot probe data. The static pressure was known not to be constant across the near wake but, as seen later in the discussion of the results, the errors caused by this simplifying assumption were not large. For the boundary-layer measurements, the surface static pressures as determined from the orifices on the airfoil's surface were used. For the wake, an approximate streamwise static-pressure distribution along the upper edge of the wake was inferred from the holographic interferometer results obtained on the DSMA 523 airfoil in Ref. 1. This distribution was in sufficiently good agreement with the distribution later obtained from laser-velocimeter, wake-edge velocity measurements that it was unnecessary to recalculate the data.

The same laser-velocimeter system discussed in Ref. 5 was used in the present experiments; consequently, the system and data-reduction procedures will only be briefly described. The velocimeter is a two-component system capable of providing simultaneous measurements of the streamwise and vertical velocity components. Both the streamwise and vertical velocity optics have Bragg-cell frequency shifting. The sensing volume of the laser velocimeter is cylindrical in shape with a diameter of approximately 0.2 mm and a length of 3 mm, the axis of the cylinder being in the cross-stream direction. Signal processing is performed with single-particle burst counters; and the individual realization from the two channels were simultaneously recorded with a digital computer. From an ensemble of at least 1000 samples of the instantaneous streamwise and vertical velocity, u_i and v_i, respectively, the mean velocities, turbulence intensities, and velocity correlations, $\overline{u'v'}$, were calculated as follows:

$$\bar{u} = \sum_{i=1}^{N} \omega_i u_i \Big/ \sum_{i=1}^{N} \omega_i \tag{1}$$

$$u' = \left(\sum_{i=1}^{N} \omega_i u_i^2 \Big/ \sum_{i=1}^{N} \omega_i - \bar{u}^2 \right)^{1/2} \tag{2}$$

$$\overline{u'v'} = \sum_{i=1}^{N} \omega_i u_i v_i \Big/ \sum_{i=1}^{N} \omega_i - \overline{uv} \tag{3}$$

In Eqs. (1-3), ω_i is the weighting factor used to account for particle arrival-rate dependency on instantaneous velocity. The two-dimensional factor

$$\omega_i = 1/(\sqrt{u_i^2 + v_i^2}) \tag{4}$$

was adopted. The equations for $\bar{v}$ and $<v'>$ are identical to Eqs. (1) and (2), except that v_i is used instead of u_i.

Naturally occurring particles in the tunnel were used as light scatterers for the velocimeter. In this facility, lubrication oil within the drive system vaporizes and later condenses in the tunnel circuit to provide a generous supply of scattering centers. Previous measurements across a normal shock have shown that these particles are small enough (estimated to be 1 μm) to give very good response to a step change in velocity at sonic speeds.

Results and Discussion

Surface and Wake-Edge Pressures

At the beginning of the test, surface-pressure data were obtained at fine increments of Mach number and angle of attack to check the sensitivity of the airfoil's performance to these parameters and to establish the test conditions for boundary-layer and wake probing. In these preliminary measurements it was also verified that the desired pressure distributions could be repeated. Off-centerline pressure taps were located on the model for checking spanwise uniformity; however, the best confirmation of two-dimensional flow was established from oil-flow visualizations at an angle of attack large enough to cause separation at the shock (i.e., a buffet condition). At this test condition, the shock location was extremely well defined by a fine line of oil buildup in the spanwise direction along the shock. The oil flow showed the shock to be farthest aft at the tunnel centerline and gradually moving forward with increasing distance from the centerline. At half a chord on either side of centerline, the shock position was less than 2% chord forward of that at centerline. The spanwise uniformity for the cruise condition would be expected to be even better.

Shown in Fig. 1 are the surface-pressure distributions for the cruise and subcritical conditions selected for boundary-layer and wake probing. Included in this figure is a sketch of the airfoil section. Since the laser-velocimeter and pitot-probe measurements were obtained during separate tunnel entries, two sets of pressure distributions are shown in Fig. 1a. One represents the nominal pressure distribution during the laser-velocimeter measurement stage of the test; the other, the nominal pressure distribution during the pitot-pressure measurement stage. As evident in this figure, the shock location was farther downstream for the pitot-probe measurements (approximately 3% chord). The distributions in Fig. 1a are representative of the average shock locations. During both the laser-velocimeter and pitot-probe phases of the test, there was some variability in shock location from one run to the next. At the extremes, the shock locations differed by approximately 3% chord. Oil-flow observations were obtained at both the cruise and subcritical test conditions. These revealed a separation bubble over approximately the last 2% chord of the airfoil for both test conditions.

Because of tunnel wall effects, the pressure distribution in Fig. 1a is not the same as would be obtained for free-air boundary conditions. Unpublished surface-pressure measurements obtained in another facility for a significantly larger chord-to-height ratio show that a lift coefficient of 0.76 can be achieved at a significantly lower angle of attack than 4.35 deg when the influence of the tunnel walls is minimized. Valid comparisons with numerical methods that predict the inviscid flow region will probably require the use of measured far-field boundary conditions such as streamwise static-pressure distributions above and below the airfoil.[6] This may not be necessary for the $M_\infty = 0.5$ test condition.

In Fig. 2, the measured surface pressures near the trailing edge for the cruise condition are shown together with the static pressures at the edge of the upper-surface boundary layer and at the upper and lower edges of the wake (as determined from velocities measured by the laser velocimeter). These latter pressures were calculated using the isentropic flow relations. A fairing of the velocimeter measurements has been made to better show the trend of the data. As seen from this figure, a static-pressure difference exists in the near wake that diminishes to zero approximately 10% chord downstream of the trailing edge. Across the upper-surface boundary layer, the static-pressure differences appear to be small, based on the measurements at the boundary-layer edge and at the surface. These observations are consistent with the observations on the DSMA 523 airfoil reported in Ref. 1, where static pressures in the inviscid flow were obtained by holographic interferometry.

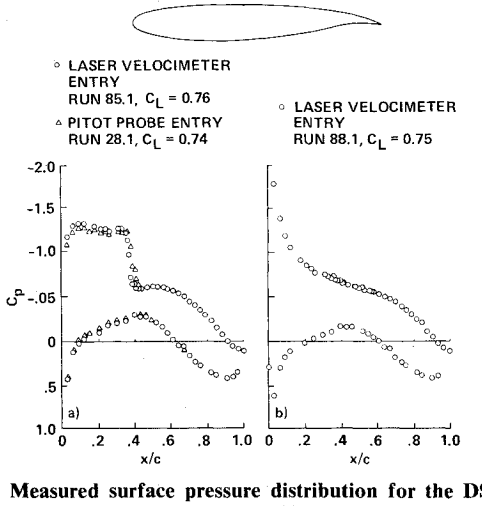

Fig. 1 Measured surface pressure distribution for the DSMA 671 airfoil section: a) $M_\infty = 0.72$, $\alpha = 4.32$ deg; b) $M_\infty = 0.5$, $\alpha = 5.35$ deg.

Notice that the pressure gradient between $x/c = 1.0$ and 1.05 at the upper edge of the wake is actually larger than it is between $x/c = 0.95$ and 1.0. The reduced pressure gradient just upstream of the trailing edge is likely a result of the small separation bubble revealed from the oil-flow visualizations.

In principle, the actual static-pressure distribution across the wake could be determined from the measurement of total pressure with the pitot probe and the velocities measured with the laser velocimeter. However, the maximum static-pressure difference observed across the wake corresponded to only a 5% jump in edge velocity. A comparison of the velocity profiles obtained immediately downstream of the trailing edge with the pitot probe (under the assumption of constant static pressure) and the laser velocimeter indicates that most of these static-pressure changes occur in the lower part of the wake; however, the differences are too subtle to infer an accurate static-pressure profile.

Local Flow Angles in the Trailing-Edge Region

Another flow property of interest in the trailing-edge region is the local flow angle. In Fig. 3, the local flow angles measured with the laser velocimeter are shown for measurement stations near the trailing edge and farther into the wake. The edges of the viscous layers are designated on each profile. At $x/c = 0.9$, the flow angles uniformly decrease across the boundary layer as the flow approaches the tangency condition near the surface. This trend was also true for all the measurement stations farther upstream. In contrast, at $x/c = 0.99$ there is a region where the flow angle increases because of the rapid growth in displacement thickness. The largest lateral flow-angle changes occur just downstream of the trailing edge, where a jump in flow angle occurs in the region where the streamwise velocity is a minimum. The flow angles at the two edges of the wake differ initially but are essentially equal at $x/c = 1.1$. Notice that the flow-angle change along the lower edge of the wake is much more gradual than that along the upper edge.

Mean-Velocity Profiles

Shown in Fig. 4 are streamwise velocity profiles measured with the pitot-pressure probe and the laser velocimeter. Along the airfoil's surface the ordinate is the vertical distance from the surface. In the wake, the ordinate is also the vertical distance but referenced to the location of the trailing edge. (To provide a clearer illustration of the results, the data at only every other vertical measurement station are shown. Also, note that different vertical scales are used for the boundary layer and the wake profiles.) The pitot-pressure probe was sufficiently small to resolve the boundary layer upstream of the shock wave. A law-of-the-wall examination of profiles measured at $x/c = 0.25$ and 0.29 stations (not shown in Fig. 4) was used to establish that the boundary layer was fully turbulent in this region. Pitot-probe measurements

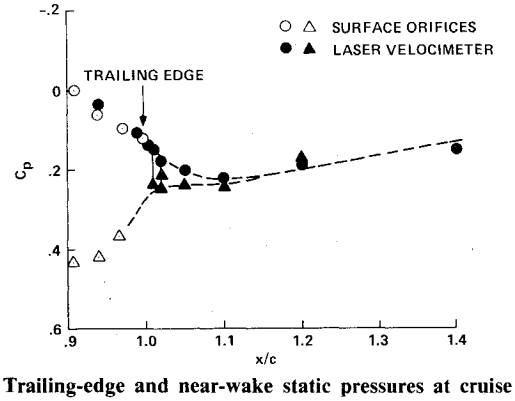

Fig. 2 Trailing-edge and near-wake static pressures at cruise condition: $M_\infty = 0.72$, $\alpha = 4.32$ deg.

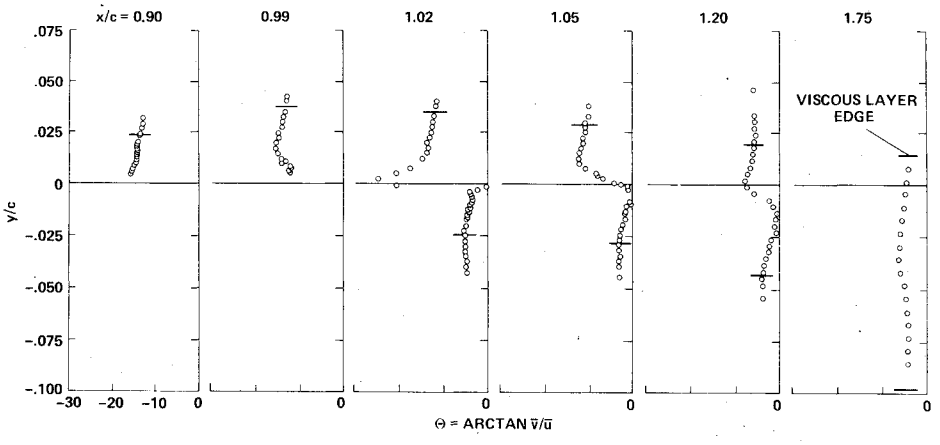

Fig. 3 Boundary-layer and near-wake flow-angle profiles at cruise condition: $M_\infty = 0.72$, $\alpha = 4.32$ deg.

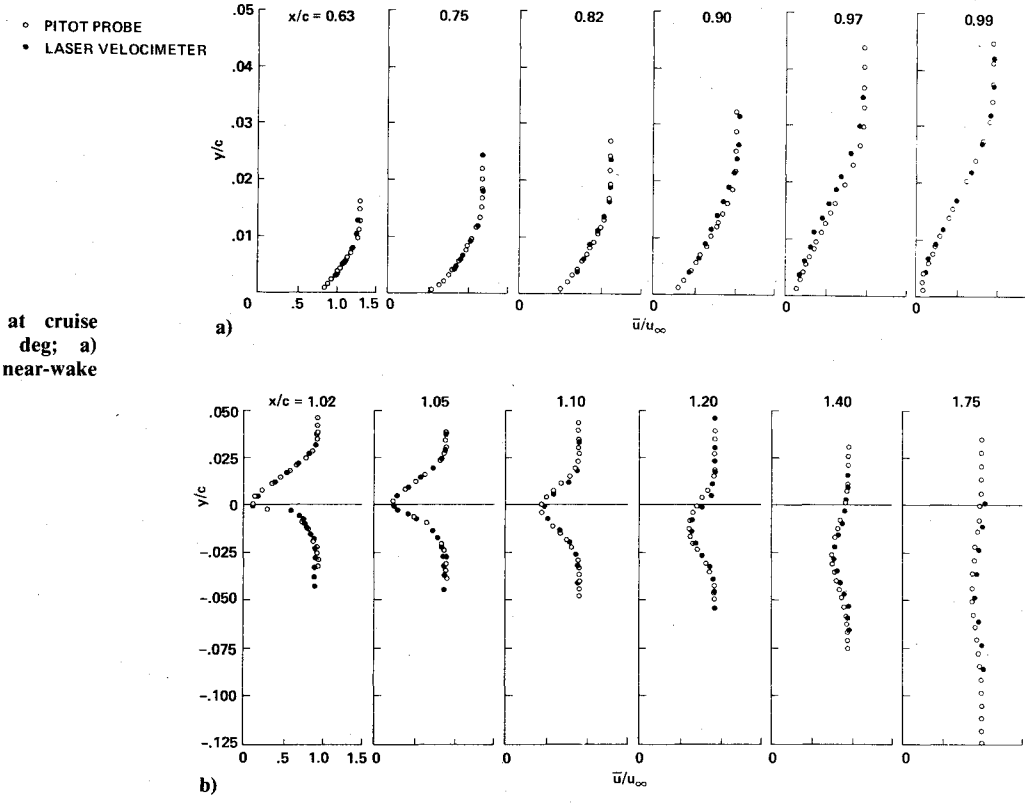

Fig. 4 Mean-velocity profiles at cruise condition: $M_\infty = 0.72$, $\alpha = 4.32$ deg; a) boundary-layer measurements; b) near-wake measurements.

between $x/c = 0.29$ and 0.62 were not taken because of the onset of vibrations in the traverse assembly when the pressure probe was in the proximity of the shock. A stiffener was added to prevent this vibration, but this produced a forward movement in the shock location. This stiffener was used only to obtain the profiles upstream of the shock.

It is evident from Fig. 4 that the pitot probe was able to provide measurements much closer to the airfoil's surface than was the laser velocimeter. Near-surface measurements with the laser velocimeter were restricted because of flare from the airfoil's surface. Had not the model been bowed, the velocimeter's performance probably would have been even more limited. At the $x/c = 0.99$ station, the boundary layer is separated; but, as seen in Fig. 5, velocimeter measurements could not be obtained sufficiently close to the surface to detect the reversed-flow region. Recall that separation occurred at approximately $x/c = 0.98$. The good agreement obtained between the two measurement techniques near the trailing edge was somewhat unexpected because of the high turbulence levels present in that region. Without the proper weighting of the laser-velocimeter results for particle arrival-rate dependency on instantaneous velocity, this agreement could not have been realized. For example, at $x/c = 1.02$, the weighted results show $\bar{u}(\text{minimum})/u_\infty = 0.10$, whereas when ω_i was taken as unity (unweighted) in the data analysis a $\bar{u}(\text{minimum})/u_\infty = 0.19$ resulted. In regions where the local turbulence levels were not as high, the differences were less.

In Fig. 5, the velocity deficit in the wake and the wake boundaries [$\bar{u} = 0.995\ u_e$ and $\bar{u} = \bar{u}(\text{minimum})$] are shown. The displacement thickness δ^*, momentum thickness θ, and shape factors H of the boundary layer and wake are shown in Fig. 6. The displacement-thickness distribution clearly illustrates the very rapid growth of the boundary layer near the trailing edge of the model. Values for the local skin-friction coefficient C_f were also obtained from least-square fits of the pitot-tube results to the law of the wall. These results are presented in a later section, where comparisons are made with boundary-layer calculations.

Turbulent-Flow Properties

Examples of the measured velocity correlation distributions, $-\overline{u'v'}/u_\infty^2$, are presented in Fig. 7. (Note that the boundary-layer and wake data are plotted on different

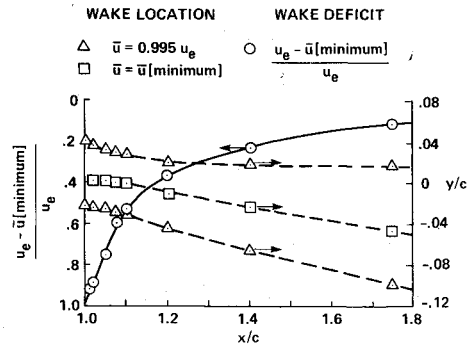

Fig. 5 Near-wake velocity deficit and boundaries at cruise condition: $M_\infty = 0.72$, $\alpha = 4.32$ deg.

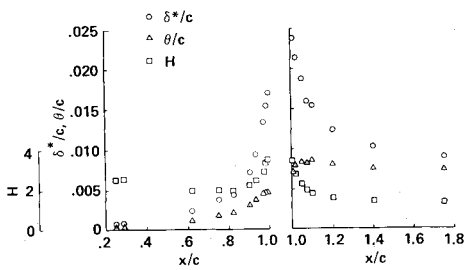

Fig. 6 Integral properties of boundary layer and near wake at cruise condition: $M_\infty = 0.72$, $\alpha = 4.32$ deg.

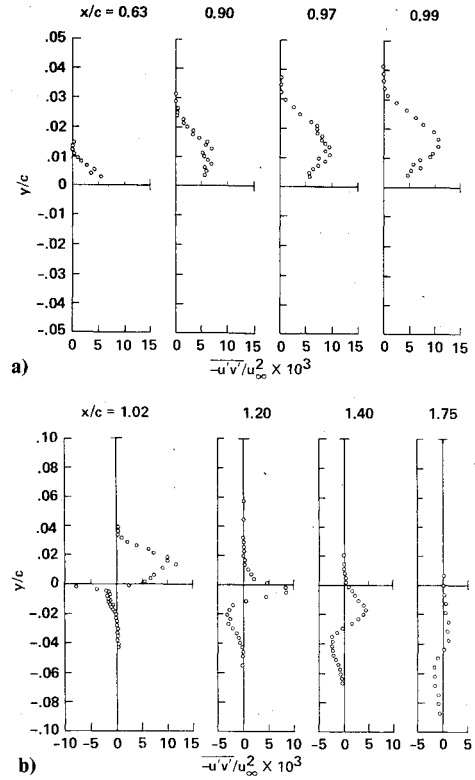

Fig. 7 Velocity correlation profiles at cruise condition: $M_\infty = 0.72$, $\alpha = 4.32$ deg; a) boundary-layer measurements, b) near-wake measurements.

vertical scales.) Since the local Mach numbers were subsonic at these measurement stations, the distribution of the nondimensional Reynolds shear stress, $-\bar{\rho}\overline{u'v'}/\rho_\infty u_\infty^2$, would be very similar to the distributions of $-\overline{u'v'}/u_\infty^2$ presented in Fig. 7. For convenience, the velocity correlation, $-\overline{u'v'}/u_\infty^2$, will be referred to as the turbulent shear stress in this paper.

The growth in the turbulent shear stress, as the flow approaches the trailing edge, followed by its subsequent decay in the wake, is evident. In Fig. 8, the turbulence intensities, $<u'>/u_\infty$ and $<v'>/u_\infty$, for the same streamwise stations are presented. Consistent with the increase in the turbulent shear stress near the trailing edge is the increase in the streamwise fluctuations in this region. Somewhat surprising, however, is the level of the vertical fluctuations at the upstream measurement stations. At these stations, the measured vertical fluctuations are of nearly the same level as the streamwise fluctuations. The correlation coefficient, $R_{uv} = \overline{u'v'}/<u'><v'>$, was near -0.5 for these measurements, which would indicate that these larger-than-expected vertical fluctuation levels were real. Since the velocity components measured were the horizontal and vertical components rather than the tangent and normal-to-the-surface components, somewhat higher vertical fluctuations should be expected. With the coordinate system used, a part of the fluctuations tangent to the airfoil's surface would appear as vertical fluctuations. However, a recalculation of the data at the $x/c = 0.62$ station for a coordinate system tangent and normal to the airfoil's surface still resulted in the vertical fluctuations being about 80% of the streamwise fluctuations. This is high compared with a zero-pressure-gradient boundary layer. This feature in the measurements is emphasized because it is pertinent to the turbulent eddy-viscosity results discussed next.

In Fig. 9, the nondimensional turbulent eddy viscosities, $\epsilon/u_e\delta_i^*$, as determined from the turbulent shear-stress measurements and the local slopes of the measured mean-velocity profiles, are presented. Along the airfoil's surface, the better resolved pitot-probe profiles were used to obtain the local slopes; in the wake, the laser-velocimeter profiles were used. Included in Fig. 9 are the eddy-viscosity distributions

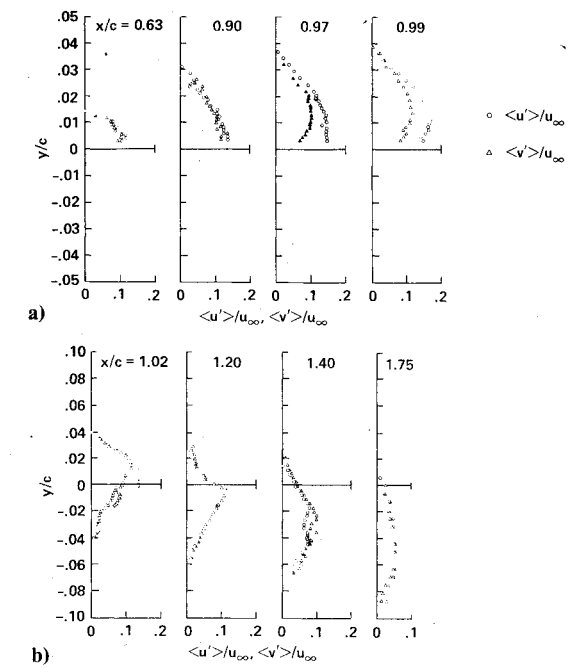

Fig. 8 Turbulence-intensity profiles at cruise condition: $M_\infty = 0.72$, $\alpha = 4.32$ deg; a) boundary-layer measurements, b) near-wake measurements.

predicted by the mixing length and Cebesi-Smith[7] formulations. The expressions used for determining the turbulent eddy viscosities were the following:

Experiment,

$$\frac{\epsilon}{u_e\delta_i^*} = -\left(\frac{\overline{u'v'}}{u_\infty^2}\right)\Big/\left(\frac{\partial(\bar{u}/u_\infty)}{\partial(y/c)}\right)\left(\frac{c}{\delta_i^*}\right)\left(\frac{u_\infty}{u_e}\right) \qquad (5)$$

Mixing length,

$$\frac{\epsilon}{u_e\delta_i^*} = \left[0.4\frac{y}{c}\left(\frac{c}{\delta}\right)\right]^2\left(\frac{\partial(\bar{u}/u_\infty)}{\partial(y/c)}\right)\left(\frac{c}{\delta_i^*}\right)\left(\frac{u_\infty}{u_e}\right) \quad (6)$$

(inner region)

$$\frac{\epsilon}{u_e\delta_i^*} = (0.09)^2\left(\frac{\partial(\bar{u}/u_\infty)}{\partial(y/c)}\right)\left(\frac{c}{\delta_i^*}\right)\left(\frac{u_\infty}{u_e}\right) \quad (7)$$

(outer region)

Cebesi-Smith,

$$\frac{\epsilon}{u_e\delta_i^*} = \left[0.4\frac{y}{c}\left(\frac{c}{\delta}\right)\right]^2\left(\frac{\partial(\bar{u}/u_\infty)}{\partial(y/c)}\right)\left(\frac{c}{\delta_i^*}\right)\left(\frac{u_\infty}{u_e}\right) \quad (8)$$

(inner region)

$$\frac{\epsilon}{u_e\delta_i^*} = 0.0168 \quad (9)$$

(outer region)

The variables on the right-hand side of Eqs. (5-8) were obtained from the experimental measurements. The boundary-layer-edge damping term $[1+5.5(y/\delta)^6]$ and the near-wall damping term normally incorporated in these two turbulence models have not been included. In the wake, only the outer-region expressions for the two turbulence models are used, with δ and δ_i^* based on the entire wake thickness.

At the upstream stations, the turbulent eddy viscosities determined from the turbulent shear-stress measurements are appreciably higher than those predicted from either of the algebraic turbulence models. The vertical fluctuations v', being larger than those for a zero pressure-gradient equilibrium boundary layer (as discussed previously), are the primary cause for the higher eddy viscosities, as compared with those predicted by the simple algebraic models. One can only speculate about the reason for the larger vertical fluctuations and, hence, higher eddy viscosities. A slow decay of the turbulence generated at the shock upstream may be the explanation. Between $x/c=0.62$ and the trailing edge, there is a definite decreasing trend in the turbulent eddy viscosity, with the data agreeing quite well with the simple algebraic models near the trailing edge. As demonstrated later, a boundary-layer calculation using the Cebeci-Smith model grossly underpredicts the boundary-layer growth near the trailing edge. A better prediction of the flow would not be expected from modifying the turbulence model in the calculation to better fit the eddy viscosities at the upstream stations. Calculators[8,9] usually resort to reducing the turbulent eddy viscosity from that predicted with the simple algebraic models in order to get a more rapid thickening of the boundary layer.

Not surprisingly, the measured and predicted turbulent eddy viscosities are in strong disagreement in the near wake (Fig. 9b). The measured turbulent eddy viscosities tend to be large near the wake center, where $\partial\bar{u}/\partial y$ is close to zero. In all cases, the shear stress and the $\partial\bar{u}/\partial y$ were of the same sign; thus no negative eddy viscosities were observed. However, care should be taken in interpreting the eddy viscosities near the wake center. With the slopes being so close to zero, a small error in the slope would have a very pronounced effect on the resultant turbulent eddy viscosity. At $x/c=1.02$ and 1.05, it is clear that neither δ nor δ_i^* of the entire wake is the appropriate length scale to use for the lower wake. The low eddy viscosities in this region reflect the much smaller length scales in this region compared with the upper wake. These smaller length scales are the remnants of the thinner boundary layer developed along the lower surface of the airfoil. By the farthest downstream station ($x/c=1.75$), this situation has changed, and the eddy viscosities are nearly equal on both sides of the wake. The inadequacies of the simple algebraic models in the near-wake region are clearly illustrated in these eddy-viscosity comparisons.

Comparison with Subcritical Test Condition Results

Laser-velocimeter measurements were also obtained at a limited number of streamwise stations between $x/c=0.9$ and 1.1 for the $M_\infty=0.5$, $C_L=0.75$ test condition. The pressure

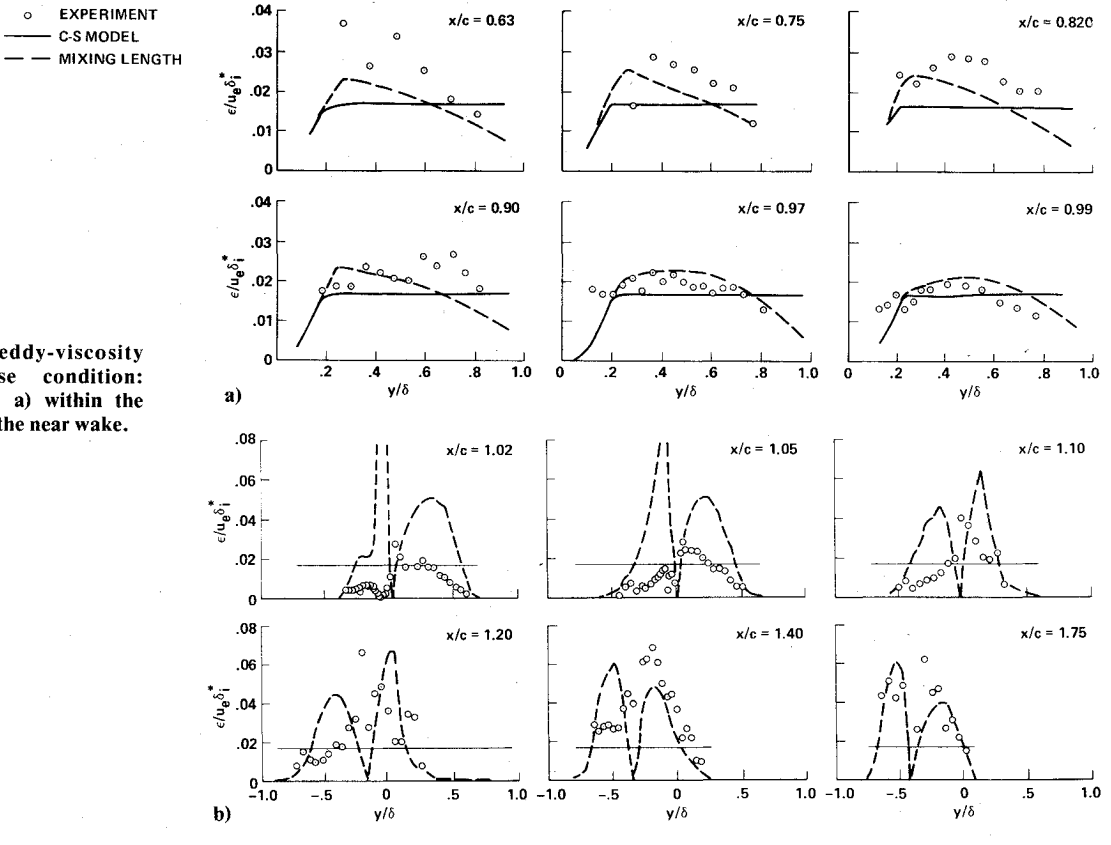

Fig. 9 Turbulent eddy-viscosity distributions at cruise condition: $M_\infty=0.72$, $\alpha=4.32$ deg; a) within the boundary layer, b) within the near wake.

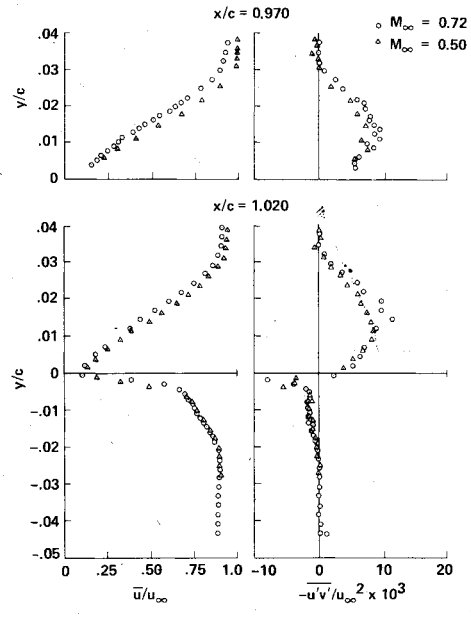

Fig. 10 Comparison of mean-velocity and velocity-correlation profiles at cruise ($M_\infty = 0.72$, $\alpha = 4.32$ deg) and subcritical ($M_\infty = 0.50$, $\alpha = 5.35$ deg) test conditions.

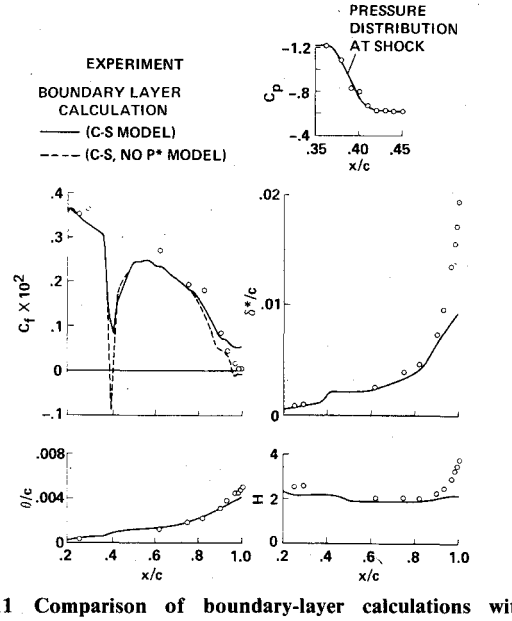

Fig. 11 Comparison of boundary-layer calculations with experimental results at cruise condition: $M_\infty = 0.72$, $\alpha = 4.32$ deg.

distribution for this test condition was presented in Fig. 1b. These measurements revealed a similar rapid growth in the boundary layer near the trailing edge. Also, the general feature of the flow near the trailing edge differed little from that at the cruise test condition. Similar static-pressure differences across the wake and flow-angle profiles were also observed. In Fig. 10, mean-velocity and turbulent shear-stress measurements obtained with the laser velocimeter are presented which illustrate the similarities of the viscous flows at these two test conditions. The results shown in Fig. 10 suggest that the steep pressure gradients along the aft portion of the airfoil and in the near wake are the controlling mechanisms for the rapid boundary-layer growth at the trailing edge. In this region, the static-pressure distributions for the subcritical and supercritical cases are nearly identical (see Figs. 1a and 1b). The shock wave present at the cruise condition appears to have been sufficiently weak that it did not significantly affect the later behavior of the boundary layer near the trailing edge. The nearly identical trailing-edge separation points for the two test conditions also support this conclusion.

Comparison with Boundary-Layer Calculations

Boundary-layer solutions were obtained for the cruise and subcritical test conditions using the inverse boundary-layer program described in Ref. 10. This program can be run in the direct mode (surface pressure specified) or inverse mode (wall shear specified). In the case in which a separation bubble is predicted, a solution is obtained for a specified wall shear by an iterative sweeping procedure which employs upwind-differencing where the flow is reversed. Since the wall shear is not known a priori, it must be guessed initially when the inverse mode is used. Once a solution is obtained for the initial guess in wall-shear distribution, the program of Ref. 10 uses an iteration procedure for updating the wall shear so as to converge to the desired pressure distribution.

Solutions were obtained using the Cebeci-Smith algebraic turbulence model (C-S model) and a modified version of this turbulence model in which the Cebeci-Smith pressure gradient correction to the Van Driest damping term was neglected (C-S, no p^* model). The solutions obtained for the cruise condition are compared with the experimental results in Fig. 11. The pressure distribution used at the shock is shown as an insert. With the removal of the pressure-gradient damping, separation was predicted at the shock and at the trailing edge, as seen from the skin-friction distribution, whereas separation was not predicted with the C-S model. But in spite of the prediction of separation with the C-S, no p^* model, it predicted essentially the same displacement thickness and shape factor distribution as the unmodified model, hence the reason for the single curves for δ^*, θ, and H in Fig. 11. The differences in the mean-velocity profiles were confined to a region so close to the airfoil's surface that the integral properties were virtually unaffected. For the calculation with separation at the trailing edge (C-S model, no p^*), iterative sweeping was only performed from just downstream of the trailing edge ($x/c = 1.01$) up to the separation point since there was no flow reversal detected in the experiments for $x/c \geq 1.01$. As seen in the comparison of displacement thicknesses, the solutions severely underpredict the growth in the boundary layer near the trailing edge. Solutions for the subcritical case[11] were in no better agreement with experiment. Calculations using the C-S model in Ref. 4 for the DSMA 523 airfoil showed a similar trend.

The reason the boundary-layer calculations fail to predict the rapid growth in displacement thickness near the trailing edge is not evident. Based on the eddy-viscosity determinations shown on Fig. 9a, it is very unlikely that it is due to inadequacies of the Cebeci-Smith model for the outer part of the boundary layer [Eq. (9)]. Since turbulent shear-stress measurements were not obtained in the near-wall region, deficiencies of this turbulence closure model for $y/\delta < 0.2$ cannot be ruled out as the cause. However, the assumption of local equilibrium upon which the Cebeci-Smith model is based should best be satisfied in the near-wall region where the turbulence scales are small. The inappropriateness of the boundary-layer approximations near the trailing edge is another distinct possibility considering the static-pressure differences and the rapid flow angle changes observed in the near wake (see Figs. 2 and 3).

Concluding Remarks

Unique viscous-flow measurements, which should aid in the development of numerical methods capable of accurately describing the flow over supercritical sections, have been presented for the upper-surface boundary layer and near wake of a supercritical airfoil section. In addition to streamwise mean velocity profiles, the data include turbulence intensity, Reynolds shear stress, and local flow angle measurements.

For both test cases (subcritical and supercritical) a small region of separated flow exists along the upper surface near the trailing edge. This small region of separated flow and the attendant rapid thickening of the upper-surface boundary layer make the test cases a formidable challenge for any predictive method. For example, a conventional boundary-layer calculation approach was shown to severely underpredict the boundary-layer growth in this region.

References

[1] Spaid, F.W. and Bachalo, W.D., "Experiments on the Flow About a Supercritical Airfoil, Including Holographic Interferometry," *Journal of Aircraft,* Vol. 18, April 1981, pp. 287-294.

[2] Melnik, R.E., Chow, R., and Mead, H.R., "Theory of Viscous Transonic Flow Over Airfoils at High Reynolds Number," AIAA Paper 77-680, 1977.

[3] Melnik, R.E., "Turbulent Interactions on Airfoils at Transonic Speeds—Recent Developments," Paper No. 10 presented at the AGARD Conference on Computation of Viscous-Inviscid Interactions; see also AGARD-CP-291, 1980.

[4] Spaid, F.W. and Stivers, L.S. Jr., "Supercritical Airfoil Boundary Layer Measurements," AIAA Paper 79-1501, 1979.

[5] Johnson, D.A. and Bachalo, W.D., "Transonic Flow About a Two-Dimensional Airfoil—Inviscid and Turbulent Flow Properties," *AIAA Journal,* Vol. 18, Jan. 1980, pp. 16-24.

[6] King, L.S. and Johnson, D.A., "Calculations of Transonic Flow About an Airfoil in a Wind Tunnel," AIAA Paper 80-1366, 1980.

[7] Cebeci, T. and Smith, A.M.O., *Analysis of Turbulent Boundary Layers,* Academic Press, New York, 1974.

[8] Deiwert, G.S., "Computation of Separated Transonic Turbulent Flows," *AIAA Journal,* Vol. 14, June 1976, pp. 735-740.

[9] Rose, W.C. and Seginer, A., "Calculation of Transonic Flow Over Supercritical Airfoil Sections," AIAA Paper 77-681, 1977.

[10] Arieli, R. and Murphy, J.D., "Pseudo-Direct Solutions to the Boundary Layer Equations for Separated Flow," *AIAA Journal,* Vol. 18, Aug. 1980, pp. 883-891.

[11] Johnson, D.A. and Spaid, F.W., "Measurements of the Boundary Layer and Near Wake of a Supercritical Airfoil at Cruise Conditions," AIAA Paper 81-1242, 1981.